Free-Space Heterochronous Imaging Reception of Multiple Optical Signals

Wei Mao and Joseph M. Kahn, *Fellow, IEEE*

Abstract—We consider free-space optical communication between a distributed collection of nodes (e.g., a distributed network of sensor nodes) and a central base station with an imaging receiver. This paper studies both synchronous and asynchronous reception of the optical signals from the nodes at the imaging receiver. Synchronous reception is done using a symbol-by-symbol maximal-ratio combining technique. We describe a low-complexity asynchronous reception scheme for the uplink that allows the nodes to transmit at a bit rate slightly lower than the frame rate. Since the two rates are nominally different, the scheme is said to be heterochronous. Our heterochronous detection algorithm uses joint maximum-likelihood sequence detection of multiple trellises, which can be implemented using the Viterbi algorithm, as well as the per-survivor processing technique. We develop an approximate upper bound for the average bit-error probability and compare it to Monte Carlo simulation results.

Index Terms—Image processing, maximum-likelihood detection (MLD), optical communication, Viterbi decoding.

I. INTRODUCTION

SENSOR NETWORKS using free-space optical communication have been proposed for several applications, including environmental monitoring, machine maintenance, and area surveillance [1]–[3]. Such systems usually consist of many distributed autonomous sensor nodes and one or more interrogating transceivers. Typically, instructions or requests are sent from a central transceiver to sensor nodes, using a modulated laser signal (downlink). In response, information is sent from the sensor nodes back to the central transceiver, using either active or passive transmission techniques (uplink). To implement active uplinks, each sensor node is equipped with a modulated laser. By contrast, to implement passive uplinks, the central transceiver illuminates a collection of sensor nodes with a single laser; the sensor nodes are equipped with reflective modulators, allowing them to transmit back to the central transceiver without supplying any optical power. As an example, Fig. 1 shows the communication architecture for Smart Dust [1], which uses passive uplinks. A modulated laser sends the downlink signals to the sensor nodes. Each sensor

node employs a corner-cube retroreflector (CCR) [1] as a passive transmitter. By mechanically misaligning one mirror of the CCR, the sensor node can transmit an on-off keyed signal to the central transceiver. While Fig. 1 shows only one sensor node, typically, there are several sensor nodes in the camera field of view (FOV). The central transceiver uses an imaging receiver, in which signals arriving from different directions are detected by different pixels, mitigating ambient light noise and interference between simultaneous uplink transmissions from different nodes (provided that the transmissions are imaged onto disjoint sets of pixels).

Optical signal reception using an imaging receiver typically involves the following four steps: first, segment the image into sets of pixels associated with each sensor, usually using some kind of training sequence; second, estimate signal and noise level in the pixels associated with each sensor; third, combine the signals from the pixels associated with each sensor, e.g., using maximal-ratio combining (MRC); last, detect and decode data. In some applications, the central transceiver transmits a periodic signal permitting the sensor nodes to synchronize their transmissions to the imaging receiver frame clock, in which case, data detection is straightforward. In other applications, especially when sensor node size, cost, or power consumption is limited, it is not possible to globally synchronize the sensor node transmissions to the central transceiver frame clock. While all the sensor nodes transmit at a nominally identical bit rate (not generally equal to the imager frame rate), each transmits with an unknown clock phase difference, i.e., the signals are *plesiochronous*. There are many existing algorithms to decode plesiochronous signals. Some algorithms involve interpolated timing recovery [4], [5], which would require considerable implementation complexity in the central transceiver. Other algorithms require the imager to oversample each transmitted bit [6], requiring the bit rate to be no higher than half the frame rate; this is often undesirable, since the imager frame rate is typically the factor limiting the bit rate, particularly when off-the-shelf imaging devices (e.g., video cameras) are used. These limitations have motivated us to develop a low-complexity decoding algorithm that allows the imaging receiver to decode signals at a bit rate just below the imager frame rate. Since the bit rate is different from the frame rate, this algorithm is said to be *heterochronous*. As we will see, this algorithm involves maximum-likelihood sequence detection (MLSD) with multiple trellises and per-survivor processing (PSP) [7].

Note that implementation of the downlink does not involve the synchronization issues just described, since each sensor node's receiver needs only to synchronize to a single received signal. In the remainder of this paper, we will focus mainly on

W. Mao is with the Department of Electrical Engineering and Computer Sciences, University of California, Berkeley, CA 94720 USA (e-mail: maowei@eecs.berkeley.edu).

J. M. Kahn was with the Department of Electrical Engineering and Computer Sciences, University of California, Berkeley, CA 94720 USA. He is now with the Department of Electrical Engineering, Stanford University, Stanford, CA 94305 USA (e-mail: jmk@ee.stanford.edu).
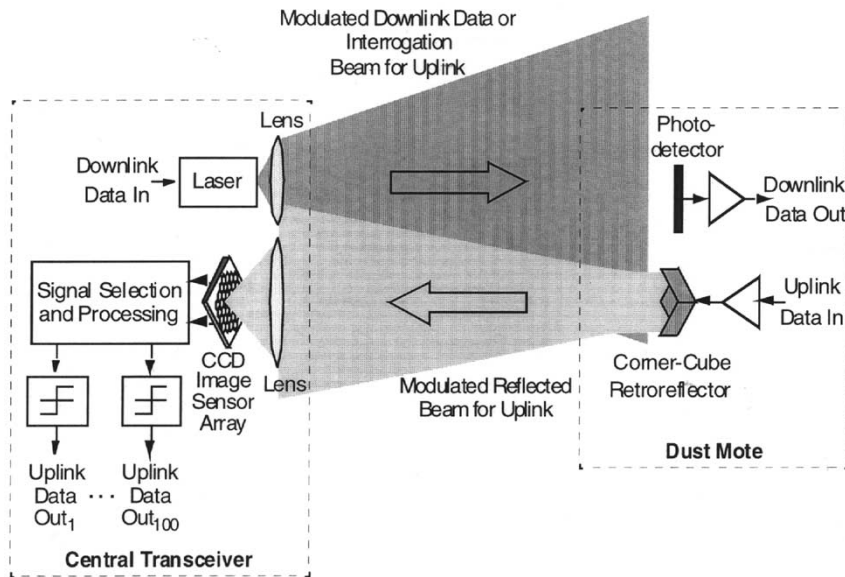
Fig. 1.   Wireless communication architecture for Smart Dust using passive optical transmitters in the sensor nodes ("dust motes").

uplink transmission. The remainder of this paper is organized as follows. In Section II, we describe the assumptions, modeling, and notation for both synchronous and heterochronous reception using an imaging receiver. In Section III, we discuss synchronous reception, including image segmentation, signal level estimation, signal combining, and detection. We describe the corresponding aspects of the heterochronous reception algorithm in Section IV. We describe an experimental system implementing the synchronous detection algorithm in Section V. In Section VI, we present our summary and conclusions.

II. SYSTEM ASSUMPTIONS AND SIGNAL MODELING

In this section, we will first state some assumptions and describe a model for the uplink as a multiple-input, multiple-output (MIMO) system. Then we will define various synchronization types to clarify some terminology used throughout this paper.

A. Uplink as a MIMO System

We assume that the transmitters use on–off keying (OOK). The instantaneous power emitted by the lth transmitter is

$$x_l(t) = \sum_k x_{l,k} A_l g_{\text{laser}}\left(t - (k-1)T - \phi_l\right) \qquad (1)$$

where $x_{l,k} \in \{0, 1\}$ is the transmitted information bit (information bits are assumed to form an independent and identically distributed (i.i.d.) sequence), A_l is the peak optical power of the lth transmitter, $g_{\text{laser}}(t)$ is a nonnegative pulse function having unit peak amplitude, T is the transmitter bit period, and ϕ_l denotes the initial time offset of the lth transmitter (typically, in practice, the time offsets of different transmitters are independent, but we do not need to make use of this assumption). Hereafter, we assume that $g_{\text{laser}}(t)$ is a rectangular pulse of duration T, i.e.,

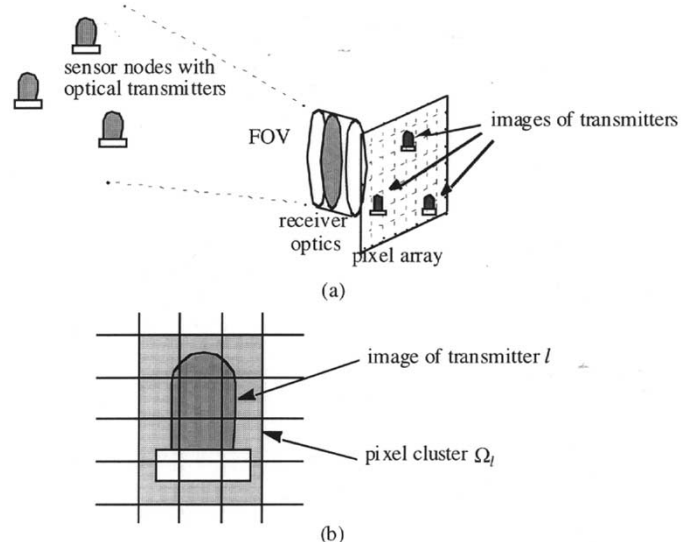$$g_{\text{laser}}(t) = \begin{cases} 1, & 0 \le t < T \\ 0, & \text{otherwise.} \end{cases} \qquad (2)$$

Fig. 2.   (a) General picture of a free-space imaging reception system consisting of sensor nodes, receiver optics, and pixel array. (b) Image of each node's transmitter falls onto several different pixels.

In this application, we can assume that the transmitters are stationary. As illustrated in Fig. 2(a), at the imaging receiver's focal plane, an image of each sensor node's optical transmitter is formed on a group of pixels that are close to each other, and each of the pixels outputs a photocurrent corresponding to the incident light intensity. In general, the collection of transmitters and pixel photocurrents form a MIMO communication system. The techniques described here are applicable as long as the images of different transmitters fall on different pixels at the receiver focal plane. This condition is usually satisfied when the number of pixels is sufficiently large, and there are a small number of transmitters within the receiver FOV.[1] Under this assumption, the re-

[1]As an example, the experimental system described in Section V uses an imaging receiver with 648×484 pixels. If five transmitters are placed at uniform, i.i.d. positions in the receiver FOV, the probability that at least two transmitters share a common pixel is only 10^{-3}.
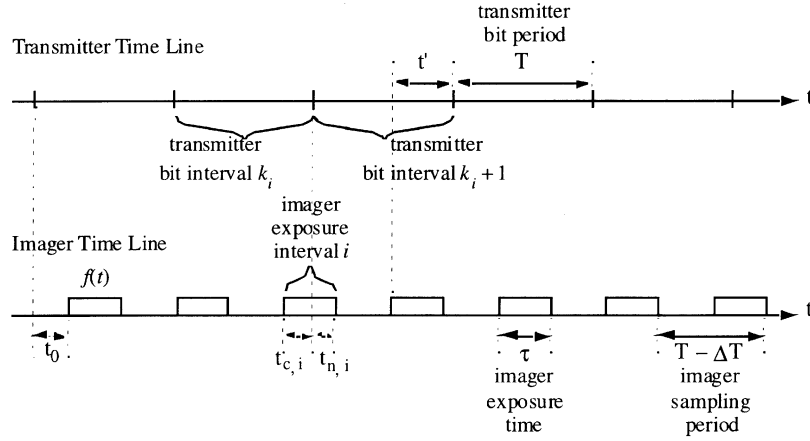
Fig. 3. Illustration of sensor node transmitter and imager time lines for heterochronous signal reception.

ceived image can be segmented into disjoint clusters of pixels, each of which contains the image of one transmitter and whose output photocurrents can be combined to detect the transmitted signal. Thus, the MIMO system naturally decomposes into a collection of uncoupled single-input, multiple-output (SIMO) systems. As shown in Fig. 2(b), we denote the cluster of pixels that contain signal $x_l(t)$ as Ω_l and let the time offset $\phi_l = 0$. We assume that the communication medium between sensor transmitters and the imaging receiver is homogenous and time invariant. The free-space channel from the lth transmitter to the mth pixel can be described as a linear time-invariant attenuation channel having impulse response $h_{l,m} \cdot \delta(t)$.[2] Our assumption of disjoint images implies that $h_{l,m} = 0$, $m \notin \Omega_l$. Since we can detect the signal from each transmitter separately, hereafter we omit the l-dependence of the pixel outputs (except in a few cases, when we include it for clarity). The signal at the output of the mth pixel ($m \in \Omega_l$) is

$$y_m(t) = x(t) \cdot h_m + d_m(t) + n_{1,m}(t) \qquad (3)$$

where $d_m(t)$ denotes the dc light level, which we can assume to be constant for the duration of the uplink communication. The term $n_{1,m}(t)$ represents the noise before light integration, including shot noise from ambient light, as well as the thermal noise from the preamplifier at each pixel. Shot noise arising from high-intensity ambient light can be modeled as white, Gaussian, and signal independent [8]. Preamplifier noise is typically Gaussian and signal independent. We model $n_{1,m}(t)$ as a zero-mean, white Gaussian noise process with double-sided power spectral density (PSD) $N_0/2$. Furthermore, $n_{1,m}(t)$ is independent of the signal and is independent (but not identically distributed) from pixel to pixel (i.e., over m).

The imaging receiver samples the signals at a frequency no lower than the transmitter bit rate. Let the imager sampling clock period be $T - \Delta T$, i.e., it is shorter than the bit period T by ΔT. During each sampling period, the imager light exposure time is

τ. The initial time offset is t_0. So the imager light exposure can be expressed as

$$f(t) = \sum_i g_{\text{shutter}}\left(t - (i-1)(T - \Delta T) - t_0\right) \qquad (4)$$

where i is an index of imager exposure intervals starting from one, and $g_{\text{shutter}}(t)$ is a nonnegative shutter pulse function with unit peak amplitude. Hereafter, we assume that $g_{\text{shutter}}(t)$ is a rectangular pulse of duration τ, i.e.,

$$g_{\text{shutter}}(t) = \begin{cases} 1, & 0 \leq t < \tau \\ 0, & \text{otherwise.} \end{cases} \qquad (5)$$

The imager light exposure function $f(t)$ is illustrated in Fig. 3 (other symbols used in Fig. 3 will be defined below). The sample at the output of the mth pixel in the ith exposure interval is

$$r_{m,i} = c_m \int_{(i-1)(T-\Delta T)+t_0}^{i(T-\Delta T)+t_0} y_m(t) \cdot f(t) dt + n_{2,m,i} \qquad (6)$$

where c_m is a constant describing the light-to-signal amplification coefficient of the mth pixel. Here, $n_{2,m,i}$ is the sample of thermal noise originating after the integrator. We assume that the $n_{2,m,i}$ are white, Gaussian, i.i.d. from time to time (i.e., over i), and also i.i.d. from pixel to pixel (i.e., over m).

The overall discrete-time noise $n_{m,i}$ in the received signal $r_{m,i}$ contains two parts. We can express it as $n_{m,i} = n_{1,m,i} + n_{2,m,i}$. The term $n_{1,m,i}$ is the noise due to shot noise and thermal noise in preamplifiers, i.e., all noise sources that originate before the integrator. It is related to $n_{1,m}(t)$ by

$$n_{1,m,i} = c_m \int_{(i-1)(T-\Delta T)+t_0}^{\tau+(i-1)(T-\Delta T)+t_0} n_{1,m}(t) dt. \qquad (7)$$

Therefore, $n_{1,m,i}$ is also white, i.i.d. from time to time (i.e., over i) and independent (but not identically distributed) from pixel to pixel. Its variance can be obtained as (omitting the time index)

$$\sigma_{1,m}^2 = E\left[\left(c_m \cdot \int_0^\tau n_{1,m}(t) dt\right)^2\right] = c_m^2 \cdot \frac{N_0}{2} \cdot \tau. \qquad (8)$$

Notice that the variance $\sigma_{1,m}^2$ is proportional to the light exposure time τ. As stated earlier, $n_{2,m,i}$ is the thermal noise added after the integrator, whose variance $\sigma_{2,m}^2$ is independent of the

imager exposure time τ. Since $n_{2,m,i}$ is independent of $n_{1,m,i}$, the overall noise $n_{m,i}$ is white and independent over m. Its variance is the sum of the variances, i.e., $\sigma_m^2 = \sigma_{1,m}^2 + \sigma_{2,m}^2$. Hereafter, we will assume that the ambient light is approximately constant within each pixel cluster, so that we can approximate $n_{m,i}$ as i.i.d. over m within a pixel cluster.

We can rewrite the received signal as

$$r_{m,i} = R_m \left(a_i \cdot x_{k_i} + b_i \cdot x_{k_i+1} \right) + d_m + n_{m,i} \qquad (9)$$

where R_m is the gain coefficient in mth pixel output, which is expressed as

$$R_m = A_l h_m c_m \cdot \tau. \qquad (10)$$

d_m is the dc signal level, a_i and b_i are linear combination coefficients (to be specified shortly). As illustrated in Fig. 3, k_i is the index of the first transmitter bit interval that overlaps with imager exposure interval i; depending on how transmitter bit k_i aligns with imager exposure interval i, transmitter bit k_i+1 may also overlap with imager exposure interval i. The imager starts with a time offset t_0 to the transmitter bits. Then $k_i = \lceil ((T - \Delta T)(i-1) + t_0)/T \rceil$. Since the bit transition can happen in the middle of the exposure period, we need to consider the imager exposure time $t_{c,i}$ to the current signal bit and the exposure time $t_{n,i}$ to the next signal bit. Let $t' = k_i T - (i-1)(T - \Delta T) - t_0$ be the time between the start of ith image reception and the end of k_ith signal bit. Then $t_{c,i} = \min(\tau, t')$ and $t_{n,i} = (\tau - t')^+$. Accordingly, $a_i = t_{c,i}/\tau$ and $b_i = t_{n,i}/\tau$. We have $a_i + b_i = 1$.

B. Definition of Various Synchronization Types

In digital system design, synchronization ensures that operations follow in the correct order. Signal reception depends greatly on whether and how the signals are synchronized. Before we make any further assumptions about the free-space communication system, it is useful to review the various types of synchronization considered in this paper.

The frequency and phase of a signal modulated by pulse-amplitude modulation (PAM) (e.g., OOK) can be defined as the frequency and phase of its associated clock. We can describe the associated clock signal as

$$p(t) = q \left((\omega + \Delta\omega)t + \theta(t) \right) \qquad (11)$$

where $q(t)$ is a precise clock signal with unit frequency and 50% duty cycle, ω is the nominal frequency of the associated clock, $\Delta\omega$ is a potential offset from the nominal frequency, and $\theta(t)$ is the instantaneous phase variation. A signal with constant average frequency, i.e., $\overline{d\theta(t)/dt} = 0$, is said to be *isochronous* [10]. Intuitively, the *anisochronous* signals are those with a time-varying frequency.

If two data signals are both isochronous with the same average frequency and instantaneous phase, then they are said to be synchronous, whereas if two signals do not satisfy those conditions, they are asynchronous. Among all forms of asynchrony, three distinct cases are of particular interest. If the signals are isochronous and have the exact same average frequency $\omega + \Delta\omega$, they are called *mesochronous*. Mesochronous signals only differ in their phases. If the average frequencies of two signals are nominally the same, but not exactly the same, these two signals are said to be *plesiochronous*. In our application, the signals
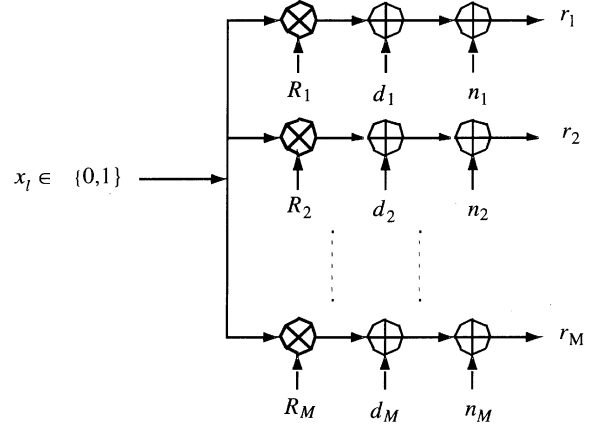

Fig. 4. SIMO communication system for synchronous reception.

from different transmitters are plesiochronous, since they share the same nominal average frequency but differ by their phases. Finally, if two signals have nominally different average frequencies, we call them *heterochronous*.

In the following two sections, we discuss methods for synchronous and heterochronous reception, respectively. Our synchronous reception method uses well-known techniques, but we will give a brief review for the sake of completeness, placing emphasis on image segmentation and signal estimation.

III. SYNCHRONOUS RECEPTION

Synchronizing the sensor nodes to the central transceiver greatly reduces the complexity of signal reception. Signal detection is done by application of MRC, which will be described in Section III-A to make clear which parameters need to be known or estimated to enable MRC. Also, in Section III-A, we present an analysis of the error probability, including the effects of errors made in estimating certain key parameters. Then in Section III-B, we describe how to segment the image and to estimate those parameters.

A. Symbol-by-Symbol MRC Detection

1) Detection Method: When the transmitters are bit synchronized to the receiver, the parameters in (9) simplify to $k_i = i$, $a_i = 1$, and $b_i = 0$. As shown in Fig. 4, the received signal can be simply expressed as

$$r_{m,i} = R_m x_i + d_m + n_{m,i}, \quad \text{for } m \in \Omega_l \qquad (12)$$

where $n_{m,i}$ is the Gaussian noise from the mth pixel, which is independent over m. Since the noise is i.i.d. over time and the signals are independently detected bit by bit, we can drop the time index i hereafter in this section. Let M denote the number of pixels in the pixel cluster Ω_l. The conditional probability density of the received signal vector $\vec{r} = (r_1, r_2, \ldots, r_M)$ from the pixel cluster given the transmitted signal can be expressed as

$$p(\vec{r}|x) = \frac{1}{\sqrt{(2\pi)^M \cdot \prod\limits_{m=1}^{M} \sigma_m^2}} \cdot \exp\left\{ -\sum_{m=1}^{M} \frac{(r_m - R_m x - d_m)^2}{2\sigma_m^2} \right\} \qquad (13)$$

where σ_m^2 denotes the variance of n_m. The maximum-likelihood detector (MLD) will pick the value of x that maximizes the likelihood of the observed signals [11]. The likelihood ratio is

$$L(\vec{r}) = \frac{p(\vec{r}|\text{on})}{p(\vec{r}|\text{off})} = \exp\left\{\sum_{m=1}^{M} \frac{R_m}{2\sigma_m^2} \cdot (2r_m - 2d_m - R_m)\right\}. \tag{14}$$

We decide that the received signal is on if $L(\vec{r}) > 1$, and otherwise, decided that it is off. So the exponent in (14) represents a set of sufficient statistics, and the MLD can be expressed as

$$\sum_{m=1}^{M} \frac{R_m}{\sigma_m^2} \cdot \left(r_m - d_m - \frac{R_m}{2}\right) \underset{\substack{< \\ \text{off}}}{\overset{\substack{\text{on} \\ >}}{\gtrless}} 0. \tag{15}$$

We weight each r_m by R_m/σ_m^2 to maximize the signal-to-noise ratio (SNR) of the weighted sum. In order to perform MRC, three quantities need to be estimated before the data reception: the gain coefficient R_m; the dc signal level d_m; and the noise variance σ_m^2. A special case occurs when the noises in the M pixels are i.i.d. Gaussian with variance σ^2, which is true in most cases, and which we assume in the remainder of this paper. In that case, the factor σ_m^2 can be dropped from the denominator, and the sufficient statistics become $\sum_{m=1}^{M} R_m \cdot (r_m - d_m - (R_m/2))$.

2) Error Probability Analysis: Estimated parameters of multiple channels are involved in this MRC detection method. First, we calculate the error probability in the absence of the parameter estimation error. The general expression for error probability for binary OOK detection is

$$P(\text{error}) = P(\text{error}|\text{on})P(\text{on}) + P(\text{error}|\text{off})P(\text{off}) \tag{16}$$

where $P(\text{error}|\text{on})$ and $P(\text{error}|\text{off})$ are the error probabilities of detecting an on or off signal, respectively, and the probabilities of receiving an on or off signal are $P(\text{on}) = P(\text{off}) = 1/2$. Let the variance of the i.i.d. Gaussian noise be σ^2. Then the overall error probability is:

$$P(\text{error}) = P(\text{error}|\text{on}) = P(\text{error}|\text{off})$$
$$= Q\left(\frac{\sum_m R_m^2}{2\sigma\sqrt{\sum_m R_m^2}}\right) \tag{17}$$

where $Q(x)$ is the Gaussian Q function [11].

Now consider the estimation error associated with parameters. The parameters involved in the MRC are R_m and $d_m + R_m/2$. Let $H_m = d_m + R_m/2$. Let $\tilde{R}_m$ and $\tilde{H}_m$ represent the estimated coefficients, and let ΔR_m and ΔH_m denote the estimation errors. Then, $\tilde{R}_m = R_m + \Delta R_m$. $\tilde{H}_m = H_m + \Delta H_m$. The two terms in (16) are no longer identical. Instead, we have

$$P'(\text{error}|\text{on}) = Q\left(\frac{\sum_m \tilde{R}_m\left(\frac{R_m}{2} + H_m - \tilde{H}_m\right)}{\sigma\sqrt{\sum_m \tilde{R}_m^2}}\right)$$
$$\approx Q\left(\frac{\sum_m R_m^2 - 2R_m\Delta H_m}{2\sigma\sqrt{\sum_m R_m^2}}\right) \tag{18}$$

$$P'(\text{error}|\text{off}) = Q\left(\frac{\sum_m \tilde{R}_m\left(\frac{R_m}{2} + \tilde{H}_m - H_m\right)}{\sigma\sqrt{\sum_m \tilde{R}_m^2}}\right)$$
$$\approx Q\left(\frac{\sum_m R_m^2 + 2R_m\Delta H_m}{2\sigma\sqrt{\sum_m R_m^2}}\right). \tag{19}$$

We have neglected the terms associated with the second- and higher-order estimation error for simplicity. We define $P' = (1/2)P'(\text{error}|\text{on}) + (1/2)P'(\text{error}|\text{off})$ to be the bit-error probability (BEP), given the estimation errors. When estimated using the method we will describe in Section III-B, the ΔR_m and ΔH_m are i.i.d. zero-mean Gaussian distributed. Therefore, the ensemble BEP is given by

$$P = \int_{\overrightarrow{\Delta H}} \int_{\overrightarrow{\Delta R}} P' \cdot p_{\overrightarrow{\Delta H}}(\overrightarrow{\Delta H}) \cdot p_{\overrightarrow{\Delta R}}(\overrightarrow{\Delta R}) \cdot d\overrightarrow{\Delta H} d\overrightarrow{\Delta R} \tag{20}$$

where $p_{\overrightarrow{\Delta H}}(\overrightarrow{\Delta H})$ and $p_{\overrightarrow{\Delta R}}(\overrightarrow{\Delta R})$ are the joint probability density functions (pdfs) of the estimation errors ΔH_m and ΔR_m, respectively. The pdfs $p_{\overrightarrow{\Delta H}}(\overrightarrow{\Delta H})$ and $p_{\overrightarrow{\Delta R}}(\overrightarrow{\Delta R})$ are products of M pdfs of zero-mean Gaussian random variables with variances σ_H^2 and σ_R^2, respectively.

To obtain an upper bound on P, we use the bound $Q(x) \leq (1/2)\exp(-x^2/2)$. Then the overall BEP is bounded by the following expression:

$$P \leq \sqrt{\frac{\sigma^2}{4(\sigma^2 + \sigma_H^2) + \sigma_R^2}} \cdot \exp\left\{-\frac{\sum_m R_m^2}{8(\sigma^2 + \sigma_H^2) + 2\sigma_R^2}\right\}. \tag{21}$$

From Section III-B, we have $\sigma_H^2 = \sigma^2/I$ and $\sigma_R^2 = 2\sigma^2/I$, where I is the number of frame samples used for parameter estimation. Hence, the BEP is bounded by

$$P \leq \sqrt{\frac{1}{4 + \frac{6}{I}}} \cdot \exp\left\{-\frac{\sum_m R_m^2}{2\sigma^2\left(4 + \frac{6}{I}\right)}\right\}. \tag{22}$$

Increasing the number of frame samples helps the detection performance. Fig. 5 shows the calculated BEP of the synchronous receiver versus the SNR, where the SNR for the lth transmitted signal is defined as

$$\text{SNR} = \frac{\sum_{m \in \Omega_I} R_m^2}{2\sigma^2}. \tag{23}$$

The dashed lines represent BEP bounds for different numbers of frame samples. The solid line corresponds to the exact BEP when parameter estimation error is absent. We observe that as I becomes larger than six, the BEP becomes relatively stable, regardless of I, and this upper bound becomes comparable to the BEP without estimation errors (17).

B. Image Segmentation and MRC Parameter Estimation

Signal recognition and image segmentation can be achieved by using a training sequence, i.e., a data sequence that is known *a priori* to the receiver. The simplest training sequence for OOK
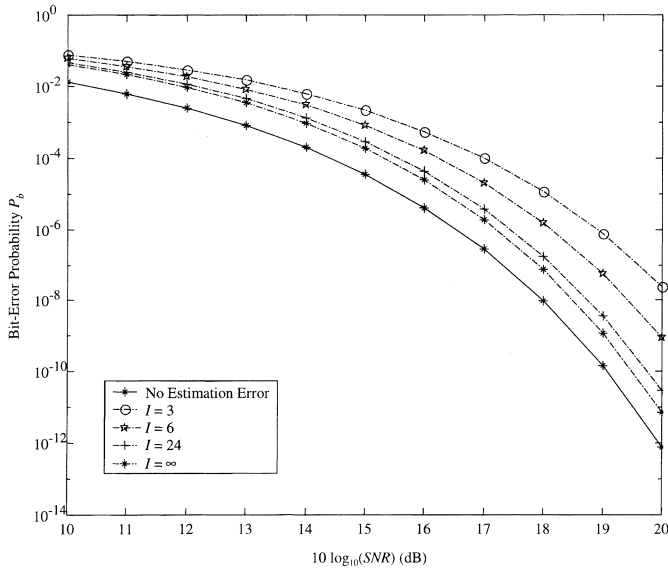
Fig. 5.   BEP of synchronous receiver versus the electrical SNR for different numbers of frame samples (I) used for parameter estimation. The solid line represents the exact error probability with no parameter estimation error, and the dashed lines are the calculated error probability bounds considering parameter estimation error.

signals is a sequence of alternating ones and zeros. Signal recognition is made based on subtraction of alternating frames and thresholding. The difference between two consecutive frames is a noisy image of the transmitted signals without the background light.

Suppose that I frames of image are taken for noise estimation, and that the noise is Gaussian and i.i.d. from pixel to pixel. Assume stationarity of the image and that the signal area is small, compared with the whole picture. Then we can treat the mth output from ith frame $r_{m,i}$ as a dc signal level d_m superimposed by a Gaussian noise n_m with variance σ^2. The dc signal level can be estimated as the time-average value of $r_{m,i}$, i.e., $\tilde{d}_m = (1/I) \sum_i r_{m,i}$. Then, a good estimate of the noise variance is the value that maximizes the likelihood of receiving $\{r_{m,i}\}$

$$\tilde{\sigma} = \arg \max_{\sigma} P\left(\{r_{m,i}\} | n_{m,i} \sim N(0, \sigma^2)\right) \qquad (24)$$

$$\tilde{\sigma} = \arg \max_{\sigma} \frac{1}{\sigma^{MI}} \cdot \exp\left\{ \frac{\sum_{i=1}^{I} \sum_{m=1}^{M} (r_{m,i} - \tilde{d}_m)^2}{2\sigma^2} \right\} \qquad (25)$$

where each $r_{m,i} = d_m + n_{m,i}$. The noise variance is estimated as

$$\tilde{\sigma}^2 = \frac{1}{MI} \cdot \sum_{i=1}^{I} \sum_{m=1}^{M} (r_{m,i} - \tilde{d}_m)^2. \qquad (26)$$

In applications where storage of the entire sequence of I frames is not possible (assuming $I > 2$), the estimation method can be slightly altered

$$2\tilde{\sigma}^2 = \frac{1}{M(I-1)} \cdot \sum_{i=1}^{I} \sum_{m=1}^{M} (r_{m,i} - r_{m,i+1})^2. \qquad (27)$$

In this case, only the consecutive frames are stored and compared. We can reuse the storage space by overwriting the older frame of the two with the newly received image frame, thereby reducing the storage space to two frames.

Assuming the images of the transmitters are convex shaped, the pixels corresponding to one transmitter are spatially connected and have a convex contour. In practice, the images are brightest at the center and become monotonically dimmer away from the center. To reduce the processing complexity, we only draw out the rectangular contour that closely covers the signal rather than identifying every single pixel, since blocks of memory are easier to index, transfer, and manipulate than clusters of individual pixels.

Under these assumptions, the following method of image segmentation has been developed. Scan the subtracted frame line by line to search for the top edge of a signal. At the detection of a first signal that does not belong to any known clusters of signal pixels, mark the y coordinate of the pixel as y_1. Then search vertically for pixels that output an above-threshold signal and note the pixel that outputs the highest value. Mark the y coordinate of the last pixel that outputs a significant value as y_2. This roughly sets the upper and lower bounds for the image segment. From the pixel that was brightest along the vertical line, search left and right for rough horizontal bounds x_1 and x_2. Depending on the shape of the sensor transmitter and light intensity distribution, refinements on the boundary may be necessary. For example, to make a refinement on the lower boundary y_2, start from the pixel which was thought to be the bottom edge of the image, perform a horizontal search for a maximum-value pixel, and search downwards for a new bound y_2'. Similar refining procedures for left and right bounds can be used. In this way, the final values of x_1, x_2, y_1, and y_2 are determined, defining the rectangular image area that contains a signal.

We direct our attention to the selected image area hereafter. Parameter estimation is achieved primarily by time averaging. The parameter $H_m = d_m + R_m/2$ is essentially the average of the light level between an on signal and an off signal. Its estimated value is the average of an even number of continuous image samples with alternating on and off signals. The estimation error ΔH_m is Gaussian with variance σ^2/I, where I is the number of samples. The gain coefficient R_m is estimated by calculating the average of differences between consecutive frame outputs. Similarly, its estimation error ΔR_m is Gaussian with variance $2\sigma^2/I$.

Among all the rectangular image areas we selected, some may be false signals caused by high noise samples. An additional stage of eliminating false image areas can be added after or during the parameter estimation. It employs MRC and current estimated parameters to check whether the signal in the pixel area is a sequence of alternating ones and zeros. Image areas that fail to output the correct training sequence are treated as false image areas and are deleted.

IV. HETEROCHRONOUS RECEPTION

As an alternative scheme to the above synchronous reception method of synchronized signals, a heterochronous reception algorithm can be implemented. In Section IV-A, we state the basic

assumptions and what needs to be prepared before reception starts. Then in Section IV-B, we describe the heterochronous reception method and perform theoretical and numerical analysis of BEP with relation to some detection parameters.

A. Basic Assumptions and Image Segmentation

We assume perfect knowledge of the transmitter bit period T, the imager bit period $T - \Delta T$, and the imager exposure time τ. Furthermore, we assume that to make efficient use of the available imager sampling frequency, $\Delta T \leq T/2$. As in the synchronous detection case, we assume that the noises are i.i.d. from pixel to pixel, with variance σ^2. As in the synchronous case, since the signals from different transmitters can be received independently, we confine discussion to reception from a single transmitter.

As shown in Fig. 3, the imager starts with an initial time offset t_0 relative to the transmitted bits; t_0 is assumed to be unknown to the receiver. We perform an initial estimation of t_0 during the training period, when an alternating one–zero sequence is transmitted, as follows. The receiver forms the difference between consecutive frames, i.e., the first difference of the received sequence. This first difference varies over time, reaching a maximum when there is no bit transition during the imager exposure interval. We record the imager exposure interval i_0 when the first difference first takes on the maximal value (after having taken on a value less than the maximum). We assume that a bit transition occurred right at the end of exposure interval $i_0 - 1$, and form our initial estimate of the time offset as

$$\hat{t}_0 = T k_{i_0} - [(T - \Delta T) \cdot (i_0 - 2) + \tau]. \quad (28)$$

When the SNR is high, the true value of t_0 lies on the interval $[\hat{t}_0 - \Delta T, \hat{t}_0 + \Delta T]$. The heterochronous reception algorithm described in the following section considers quantized candidate values of t_0 lying on that interval, and forms a more refined estimate of t_0. When the SNR is low, it is possible that the true value of t_0 might deviate from the initial estimate $\hat{t}_0$ by more than ΔT. In that case, we can extend the algorithm described in the following section to consider a wider range of candidate values of t_0 in refining the estimate of t_0.

Image area selection can be done in a manner similar to the synchronous case. Since maximal contrast between two adjacent frames is not achieved during all frames due to asynchrony, a larger number of frames are needed for refinement of image locations. The dc light level d_m in each pixel, which must be estimated to perform detection, can be estimated accurately before the training sequence starts. However, estimation of the gain coefficient in each pixel, R_m, is complicated by the intersymbol interference (ISI) in the received signals. For each pixel, only a rough estimation can be obtained by taking the maximum value of the first difference over time. This estimate of R_m is needed as the initial value of R_m for further refinement. Then we can estimate the R_m more accurately during data detection using PSP.

B. Heterochronous MLSD Reception Using Extended Trellis Diagram and PSP

1) Description of the Algorithm: As stated in Section II, if the transmitted sequence of bits is $\{x_k\}$, the received signal is

$$r_{m,i} = R_m \left(\frac{t_{c,i}}{\tau} \cdot x_{k_i} + \frac{t_{n,i}}{\tau} \cdot x_{k_i+1} \right) + d_m + n_{m,i} \quad (29)$$

where the parameters are defined in Section II and illustrated in Fig. 3. Suppose that I frames of images were received. The conditional probability density of the received signal $\vec{r} = (r_{1,1}, \ldots, r_{M,1}, \ldots, r_{1,I}, \ldots, r_{M,I})$, given the transmitted bit sequence $\vec{x} = (x_1, \ldots, x_{k_I+1})$, is given by

$$p(\vec{r}|\vec{x}) = \frac{1}{\sqrt{(2\pi\sigma^2)^{IM}}}$$

$$\cdot \exp \left\{ -\frac{1}{2\sigma^2} \left(r_{m,i} - d_m - R_m \left(\frac{t_{c,i}}{\tau} x_{k_i} + \frac{t_{n,i}}{\tau} x_{k_i+1} \right) \right)^2 \right\}. \quad (30)$$

Given a received signal $\vec{r}$, we would like to estimate the transmitted bit sequence using MLSD, i.e., by determining the bit sequence $\vec{x}$ that minimizes the correlation metric

$$\Gamma = \sum_{i=1}^{I} \sum_{m=1}^{M} \left(r_{m,i} - d_m - R_m \left(\frac{t_{c,i}}{\tau} x_{k_i} + \frac{t_{n,i}}{\tau} x_{k_i+1} \right) \right)^2. \quad (31)$$

In principle, this MLSD can be implemented using the Viterbi algorithm. However, performing MLSD is complicated by uncertainty in the initial time offset t_0 and in the gain coefficients R_m.

As stated in the previous section, our initial estimate $\hat{t}_0$ of the starting time offset t_0 is uncertain; the actual value of t_0 lies within the interval $[\hat{t}_0 - \Delta T, \hat{t}_0 + \Delta T]$. To combat this uncertainty, we quantize t_0 into several values that are uniformly spaced on that interval. Instead of performing MLSD on a single trellis, we perform MLSD on one trellis for each quantized value of t_0. We jointly estimate the bit sequence $\vec{x}$ and the time offset t_0 by determining the joint values that minimize the correlation metric (31).

Also, as stated in the previous section, it is difficult to estimate the gain coefficients R_m prior to MLSD. To combat this uncertainty, we employ suboptimal PSP [7]. The key idea of PSP is to calculate metrics for a transition in the trellis, using estimates of the unknown quantities corresponding to the data sequence associated with the survivor path leading to that transition. Suppose that for a particular transition, we have a sequence of tentative decisions denoted by $\{\hat{x}_k\}_{k=1}^{l}$. Then a data-aided parameter estimator provides the Viterbi decoder with an estimate of the gain coefficients as

$$\widetilde{R}_{m,l} = \frac{\displaystyle\sum_{i=1}^{I_l} (r_{m,i} - d_m)}{\displaystyle\sum_{i=1}^{I_l} \left(\frac{t_{c,i}}{\tau} \hat{x}_{k_i} + \frac{t_{n,i}}{\tau} \hat{x}_{k_i+1} \right)} = \frac{\displaystyle\sum_{i=1}^{I_l} (r_{m,i} - d_m)}{\frac{t_{c,1}}{\tau} \hat{x}_1 + \frac{t_{n,I_l}}{\tau} \hat{x}_l + \displaystyle\sum_{k=2}^{l-1} \hat{x}_k} \quad (32)$$

where I_l is the number of received signals when the sequence of tentative decisions of length l is made.

2) Error Probability Analysis: To simplify the analysis, we assume that the gain coefficients R_m are estimated with negli-

gible error. This assumption is verified below by comparison of our error probability analysis with Monte Carlo simulation results. Let the transmitted bit sequence be $\overrightarrow{X^{(0)}}$ and the Viterbi decoded sequence be $\overrightarrow{X^{(1)}}$. Let q denote the number of quantization levels used to estimate the starting time offset t_0. We assume that the decoder's estimate of t_0 is the quantized value closest to the true value of t_0. In this case, the estimation error of t_0, denoted by Δt_0, is uniformly distributed on the interval $[-\Delta T/q, \Delta T/q]$. Assuming that t_0 is uniformly distributed on the interval $[0, T - \Delta T]$, an upper bound for the average BEP is expressed by

$$P_b < \lim_{K \to \infty} \frac{1}{K} \sum_{\substack{\overrightarrow{X^{(0)}}, \overrightarrow{X^{(1)}} \in E \\ \overrightarrow{X^{(1)}} \neq \overrightarrow{X^{(0)}}}} w\left(\overrightarrow{X^{(1)}} - \overrightarrow{X^{(0)}}\right) \cdot P\left(\overrightarrow{X^{(0)}}\right)$$

$$\cdot \left[\frac{1}{T - \Delta T} \cdot \frac{q}{2\Delta T} \right.$$

$$\cdot \int_0^{T-\Delta T} \int_{-\frac{\Delta T}{q}}^{\frac{\Delta T}{q}} P\left(\text{favor}\overrightarrow{X^{(1)}} | \overrightarrow{X^{(0)}}; t_0, \Delta t_0\right)$$

$$\left. \cdot d\Delta t_0 \cdot dt_0 \right]. \tag{33}$$

Here, $w(\vec{e})$ denotes the Hamming weight of the error sequence $\vec{e}$, which is the difference between $\overrightarrow{X^{(0)}}$ and $\overrightarrow{X^{(1)}}$, K is the length of the sequences $\overrightarrow{X^{(0)}}$ and $\overrightarrow{X^{(1)}}$, and E is the set of all possible sequences $\overrightarrow{X^{(0)}}$ and $\overrightarrow{X^{(1)}}$.

The term $P(\text{favor}\overrightarrow{X^{(1)}} | \overrightarrow{X^{(0)}}; t_0, \Delta t_0)$ is the probability that the Viterbi decoder favors sequence $\overrightarrow{X^{(1)}}$ when sequence $\overrightarrow{X^{(0)}}$ is transmitted, assuming t_0 and Δt_0 are known. This event occurs when $\overrightarrow{X^{(1)}}$ produces a smaller value of (31) than $\overrightarrow{X^{(0)}}$ does. Let $S_{m,i}(\overrightarrow{X})$ be the signal expected in the ith exposure interval when the bit sequence $\overrightarrow{X}$ is transmitted, i.e.,

$$S_{m,i}(\overrightarrow{X}) = R_m \left(\frac{t_{c,i}}{\tau} x_{k_i} + \frac{t_{n,i}}{\tau} x_{k_i+1} \right). \tag{34}$$

Similarly, we can define $S'_{m,i}(\overrightarrow{X})$ to be the corresponding expected signal using the estimated value of t_0. Then we have

$$P\left(\text{favor}\overrightarrow{X^{(1)}} | \overrightarrow{X^{(0)}}; t_0, \Delta t_0\right) = Q\left(\frac{\sqrt{\sum_m \sum_i S'_{m,i}(\vec{e})^2}}{2\sigma} \right.$$

$$\left. + \frac{\sum_m \sum_{i \in I^*} 2S'_{m,i}(\vec{e}) \left(S'_{m,i}\left(\overrightarrow{X^{(0)}}\right) - S_{m,i}\left(\overrightarrow{X^{(0)}}\right) \right)}{2\sigma\sqrt{\sum_m \sum_i S'_{m,i}(\vec{e})^2}} \right) \tag{35}$$

where I^* denotes the set of time indexes where ISI is present. In the argument of the Q function, the first term represents the performance in the absence of ISI (dependent solely upon the SNR), while the second term represents the asynchronous penalty due to ISI. The derivation now proceeds in two steps: first, approximate the double integral inside

the square brackets of (33) by taking the maximum value of $P(\text{favor}\overrightarrow{X^{(1)}} | \overrightarrow{X^{(0)}}; t_0, \Delta t_0)$ over t_0 and Δt_0, denoted by $\hat{P}(\text{favor}\overrightarrow{X^{(1)}} | \overrightarrow{X^{(0)}}; t_0, \Delta t_0)$; then, keep the dominant terms in the summation, which are the terms corresponding to $w(\overrightarrow{X^{(1)}} - \overrightarrow{X^{(0)}}) = 1$, and calculate the summation. With the additional assumption that ΔT is small compared to τ, the following approximate upper bound is obtained:

$$P_b \leq Q\left(\frac{\sqrt{\sum_m R_m^2}}{2\sigma} \cdot \frac{\Delta T + \tau}{\sqrt{2}\tau} \cdot \left(1 - \frac{2}{q} \cdot \frac{\Delta T}{\Delta T + \tau}\right) \right). \tag{36}$$

Observe that in the argument of the Q function, the first factor represents the effect of the SNR, while the remaining factors approximate the SNR penalty caused by asynchronous ISI. We define the factor

$$\Pi = \frac{(\Delta T + \tau)^2 \cdot \left(1 - \frac{2}{q} \cdot \frac{\Delta T}{\Delta T + \tau}\right)^2}{2\tau^2} \tag{37}$$

and note that in the presence of asynchronous ISI, to maintain a given error probability, the SNR must be increased approximately by a factor $\Pi^{-1} > 1$, i.e., the SNR penalty in decibels is approximately $-10\log_{10}\Pi > 0$. This penalty is most easily interpreted in the case when q is large, so the effect of inaccurate estimation of the initial time difference t_0 is eliminated. In this case, $\Pi \to 1/2(1 + (\Delta T/\tau))^2$, and the ISI penalty becomes solely dependent on $(\Delta T/\tau)$. Since asynchronous ISI cannot increase detection efficiency, (37) can be valid only when $\Pi \leq 1$, i.e., when $(\Delta T/\tau) \leq \sqrt{2} - 1$. In the limit that $(\Delta T/\tau) \ll 1$, the ISI penalty approaches 3 dB.

We have performed Monte Carlo simulations using MATLAB in order to test the accuracy of the error-probability bound (36). The transmitter emits pseudorandom bit sequences at a bit rate of 50 b/s, i.e., $T = 20$ ms. The imager sampling frequency is higher than 50 Hz, and the imager sampling interval is $T - \Delta T$ ms. The transmitter's image is distributed among 10 adjacent pixels with light intensities proportional to $\{10, 9, 9, 8, 8, 7, 7, 6, 6, 5\}$, respectively. These intensities are estimated initially with random deviations within 10% to their correct values. PSP estimates gain coefficients $\tilde{R}_m$ at every step of MLSD based on prior bit decisions in the surviving path. We average results of simulations with five initial time offsets t_0 equally spaced between 0 and 19 ms.

First, we investigate the effect of q, the number of quantization levels of the initial estimate of t_0. We set $\Delta T = 1$ ms, i.e., the imager sampling period is 19 ms. The imager exposure time τ is fixed to be 10 ms. We vary the electrical SNR from 7 to 16 dB, and plot the simulation results along with the approximate upper bound (36). As shown in Fig. 6, the two solid lines represent simulation results with $q = 2$ and 16, and the three dashed lines represent evaluation of (36) for $q = 2$, 16, and ∞, respectively. The bound (36) is pessimistic for $q = 2$, and is tight for $q > 2$. There is only a half-decibel difference at high SNR between the bound and the simulated results for $q = 16$. Most importantly, the simulated performance is almost independent of q for $q > 2$. Hence, the performance of the heterochronous
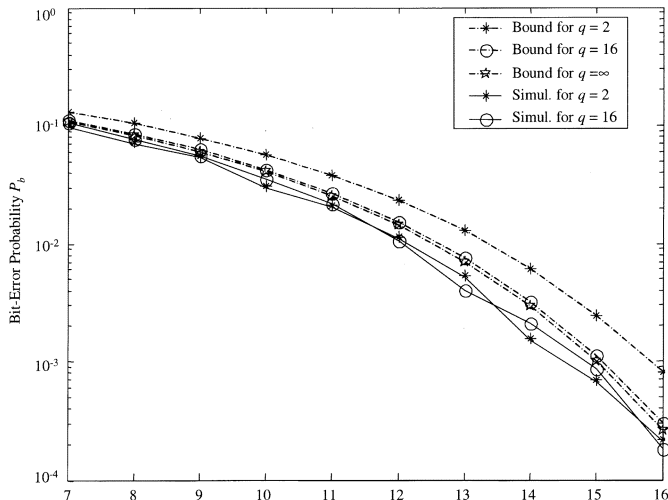
Fig. 6. Ensemble-average BEP of multiple-trellis MLSD receiver versus the electrical SNR for different quantization levels q of the initial time difference t_0. Transmitter bit period $T = 20$ ms, bit period difference $\Delta T = 1$ ms, and light exposure time $\tau = 10$ ms are assumed. The dashed lines represent the approximate upper bound (36), and the solid lines represent Monte Carlo simulations.
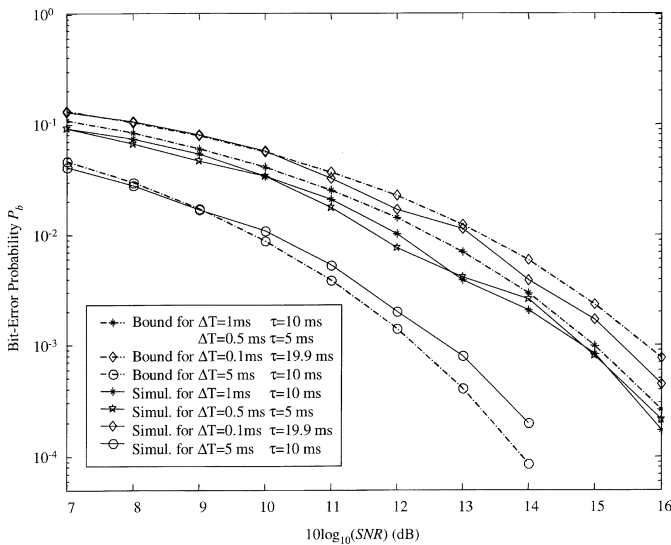

Fig. 7. Ensemble-average BEP of multiple-trellis MLSD receiver versus the electrical SNR for different values of the bit period difference ΔT and the light exposure time τ. We assume a transmitter bit period $T = 20$ ms, and $q = 2$ quantization levels of the initial time difference t_0. Dashed lines represent the approximate upper bound (36), while solid lines represent Monte Carlo simulations.

receiver is insensitive to the choice of q, and the choice $q = 2$ is sufficient to obtain good performance, in practice.

We now study the accuracy of the bound (36) for different values of ΔT and τ. The system setup is as described just above, except that we fix $q = 2$ and choose the values ($\Delta T = 1$ ms, $\tau = 10$ ms), ($\Delta T = 0.5$ ms, $\tau = 5$ ms), ($\Delta T = 0.1$ ms, $\tau = 19.9$ ms), and ($\Delta T = 5$ ms, $\tau = 10$ ms). We vary the electrical SNR from 7 to 16 dB. In Fig. 7, we plot the Monte Carlo simulation results using solid lines and plot the approximate upper bound (36) using dashed lines. Since the approximate upper bound (36) is tight for large q, we choose $q = \infty$ in plotting (36) in Fig. 7. The first two sets of parameters produce
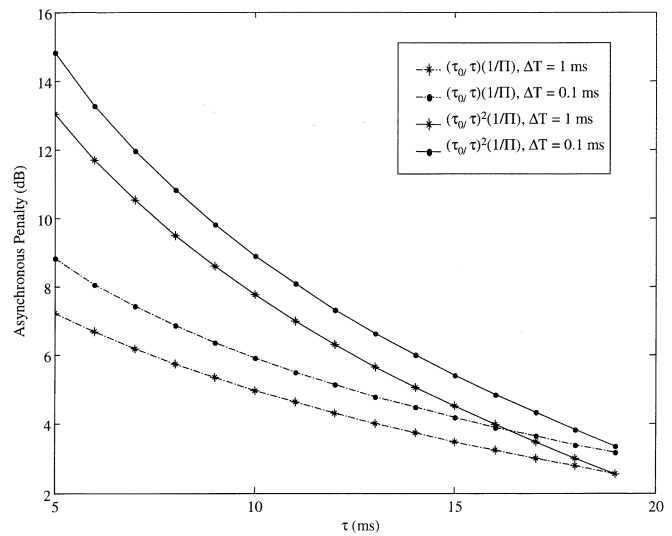

Fig. 8. Overall asynchronous penalty (SNR penalty plus ISI penalty) of the multiple-trellis MLSD receiver versus the light exposure time τ for different noise regimes and difference values of the bit period difference ΔT. Transmitter bit period $T = 20$ ms and $q = \infty$ quantization levels of the initial time difference t_0 are assumed. The dashed lines represent the penalty when ambient light shot noise and thermal noise in the preamplifier dominate. The solid lines represent the penalty when thermal noise originating after the integrator dominates.

the same ratio $(\Delta T/\tau)$, and are thus described by a common approximate upper bound; their Monte Carlo simulations are quite similar to each other and differ by about a half decibel from that common bound. Simulations for the third set of parameters show that the bound (36) is tight when $(\Delta T/\tau) \ll 1$. Results for the fourth set of parameters confirm that when $(\Delta T/\tau) > \sqrt{2} - 1$, the bound (36) is optimistic.

It is worth mentioning that the good agreement between our Monte Carlo simulations and the bound (36) implies that PSP performs well in estimating the gain coefficients R_m.

As stated previously, the asynchronous ISI penalty depends on the ratio $\Delta T/\tau$. For a fixed set of physical link parameters (transmission distance, ambient light intensity, etc.), increasing τ increases the SNR.[3] Let us consider how the overall performance depends on the choice of τ. We define τ_0 to be the largest possible value of τ, i.e., $\tau_0 = T - \Delta T$. It is necessary to consider two different noise regimes. First, when ambient light shot noise and thermal noise in the preamplifier dominate, the noise variance is proportional to τ, and the overall SNR is proportional to τ. When $\tau < \tau_0$, the SNR penalty is $\tau_0/\tau > 1$, and the overall penalty (SNR plus ISI) is $\tau_0/\tau\Pi^{-1}$. Second, when thermal noise originating after the integrator dominates, the noise variance is independent of τ, and the overall SNR is proportional to τ^2. When $\tau < \tau_0$, the SNR penalty is $(\tau_0/\tau)^2 > 1$, and the overall penalty (SNR plus ISI) is $(\tau_0/\tau)^2\Pi^{-1}$. In Fig. 8, we plot examples of the overall penalty in the two noise regimes. We assume $T = 20$ ms, consider $\Delta T = 0.1$ ms and 1 ms, and vary τ between 5 and 19 ms. The dashed lines represent the regime when noise originating before the integrator dominates, and the solid lines represent the regime when noise originating after the integrator dominates. At small values of τ, the second noise regime

[3]Choosing larger τ can also minimize the impact of the finite rise and fall times of the transmitted signal and of the imager exposure interval.
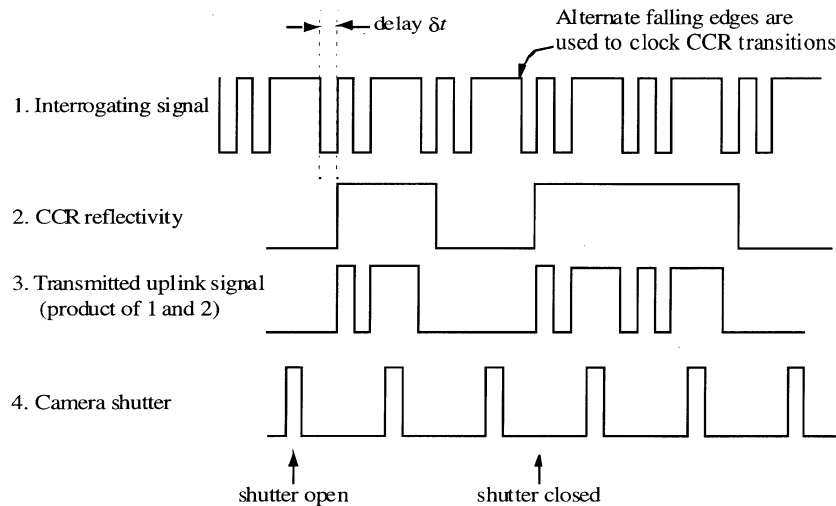
Fig. 9.   Synchronization of central transceiver and dust motes during uplink transmission.

yields larger total penalties than the first noise regime. Clearly, in both regimes, it is advantageous to choose τ to be as large as possible.

V. EXPERIMENTAL SYSTEM

As part of the Smart Dust project [2], we have built a free-space optical communication system for sensor networks using the synchronous detection method described in Section III. The system transmits to and receives from miniature sensor nodes, which are called "dust motes." The early prototype system described here achieves a downlink bit rate of 120 b/s, an uplink bit rate of 60 b/s, and a range of up to 10 m. A more recent prototype system [13] has achieved an increased uplink bit rate of 400 b/s and an increased range of 180 m.

Fig. 9 shows an overview of the communication architecture.

Each dust mote is equipped with a power supply, sensors, analog and digital circuitry, and optical transmitter and receiver. The dust mote receiver comprises a simple photodetector and preamplifier. The dust mote transmits using a CCR [13], which transmits using light supplied by an external interrogating laser. A CCR is comprised of three mutually perpendicular mirrors, and reflects light back to the source only when the three mirrors are perfectly aligned. By misaligning one of the CCR mirrors, the dust mote can transmit an OOK signal.

The central transceiver is equipped with a 532-nm (green) laser having peak output power of 10 mW. The laser beam is expanded to a diameter of 2 mm, making it Class 3A eye-safe [12]. At the plane of the dust motes (typically 10 m from the transceiver), a spot of 1 m radius is illuminated, and dust motes within the beam spot can communicate with the transceiver. The laser serves both as a transmitter for the downlink (transceiver to dust motes) and as an interrogator for the uplink (dust motes to transceiver). For downlink transmission, the laser can be modulated using OOK at a bit rate up to 1000 b/s (the dust mote receiver limits the downlink bit rate to 120 b/s). During uplink transmission, the laser is also modulated to permit the dust motes to synchronize their transmissions. The central transceiver is equipped with a progressive-scan 648 × 484 pixel charge-coupled device (CCD) camera and frame grabber. The frame grabber rate of 60

frame/s limits the uplink bit rate. Fig. 9 shows how the modulated interrogating beam is used to synchronize CCR transitions to the camera frame clock during uplink transmission. The dust mote receiver detects the modulated interrogating beam and synchronizes CCR transitions at an appropriate fixed time delay δt after alternate falling edges. The frame grabber captures images and transfers them to a personal computer. A program in the C language performs image segmentation, MRC parameter estimation, and MRC detection.

VI. CONCLUSIONS

The free-space optical communication systems with sensor networks are widely used in many applications. We have found that the communication architecture is straightforward and robust if the transmissions from all the sensor nodes are bit synchronized to the receiver imager array. The signal can be decoded by using modified MRC of the relevant pixel outputs. Training sequence can be employed before the data transmission to assist in estimating the parameters of MRC. In order to achieve this synchronization, the central transceiver must transmit an interrogating signal, which all of the sensor nodes must receive and synchronize to, e.g., using a phase-locked loop. Constraints on the size and power consumption of sensor nodes may make it difficult to implement this synchronous communication architecture. So it is desirable to relax the requirement for the dust motes to be synchronized to the imager.

In this paper, we developed an asynchronous detection algorithm permitting the sensor nodes to transmit at a bit rate approaching the frame rate. We assume that all sensor nodes transmit at an nominally identical bit rate, which is known to the receiver. When the sensor nodes transmit heterochronously to the imager array, during each frame interval, the imager sample is a linear combination of two adjacent bits, which can be treated as a form of ISI. Our heterochronous detection algorithm uses MLSD, which can be implemented using the Viterbi algorithm.

This heterochronous detection algorithm requires estimation of the starting time offset between the sensor signal and the imager sampling signal. A rough estimation can be made to

decide this starting time offset, then this estimation is quantized to a precision of several time slots per bit interval. In this MLSD algorithm, we use multiple trellis corresponding to different values of the starting time offset and make joint decisions based upon the extended trellis diagram. In addition, the receiver needs to estimate pixel combining weights for MRC; these are estimated by incorporated PSP in the MLSD algorithm.

An approximate upper bound for the average BEP is derived. Monte Carlo simulation results show that this bound is pessimistic for small quantization levels of the starting time offset ($q = 2$), and is tight for large q. The simulated performance is insensitive to the choice of q, and the choice $q = 2$ is sufficient to obtain good performance, in practice. Simulation results also show that the bound is tight when the ratio $(\Delta T)/\tau \ll 1$. Good agreement between simulations and the bound implies that PSP performs well in estimating the gain coefficients. The study also proves that choosing the light exposure time τ as large as possible can help reduce the asynchronous penalty.

ACKNOWLEDGMENT

REFERENCES

[1] J. M. Kahn, R. H. Katz, and K. S. J. Pister, "Emerging challenges: mobile networking for smart dust," *J. Commun., Networks*, vol. 2, no. 3, pp. 188–196, Sept. 2000.

[2] B. A. Warneke, M. D. Scott, B. S. Leibowitz, L. Zhou, C. L. Bellew, J. A. Chediak, J. M. Kahn, B. E. Boser, and K. S. J. Pister, "An autonomous 16 mm^3 solar-powered node for distributed wireless sensor networks," in *Proc. IEEE Sensors 2002 Conf.*, Orlando, FL, June 12–14, 2002, pp. 1510–1515.

[3] P. F. Szajowski, G. Nykolak, J. J. Auborn, H. M. Presby, and G. E. Tourgee, "High power optical amplifier enabled 1550 nm terrestrial free-space optical data-link operating at 10 Gb/s," in *Proc. IEEE Military Communications Conf.*, Atlantic City, NJ, Oct. 31–Nov. 3, 1999, pp. 687–689.

[4] M. Spurbeck and R. T. Behrens, "Interpolated timing recovery for hard disk drive read channels," in *Proc. Int. Conf. Communications*, New York, NY, 1997, pp. 1618–1624.

[5] T. Oenning and J. Moon, "Digital detection with asynchronous sampling using amplitude error prediction," *IEEE Trans. Magn.*, vol. 34, pp. 1931–1933, July 1998.

[6] C. Bertrand and P. Sehier, "A novel approach for full digital modems implementing asynchronous sampling techniques," in *Proc. IEEE Globecom*, vol. 2, New York, NY, 1996, pp. 1320–1324.

[7] R. Raheli, A. Plydoros, and C. Tzou, "Per-survivor processing: a general approach to MLSE in uncertain environments," *IEEE Trans. Commun.*, vol. 43, pp. 354–364, Feb.–Apr. 1995.

[8] J. M. Kahn and J. R. Barry, "Wireless infrared communications," *Proc. IEEE*, vol. 85, pp. 265–298, Feb. 1997.

[9] X. Zhu and J. M. Kahn, "Maximum-likelihood spatial-diversity reception on correlated turbulent free-space optical channels," in *Proc. IEEE Conf. Global Telecommunications*, San Francisco, CA, Nov. 27–Dec. 1, 2000, pp. 1237–1241.

[10] D. G. Messerschmitt, "Synchronization in digital system design," *IEEE J. Select. Areas Commun.*, vol. 8, pp. 1404–1419, Oct. 1990.

[11] J. G. Proakis, *Digital Communications*, 3rd ed. New York: McGraw-Hill, 1995.

[12] International Electrotechnical Commission, CEI/IEC825-1: Safety of Laser Products, 1993.

[13] L. Zhou, J. M. Kahn, and K. S. J. Pister, "Corner-cube retroreflectors based on structure-assisted assembly for free-space optical communication," *J. Microelectromech. Syst.*, vol. 12, pp. 233–242, June 2003.

Wei Mao received the B.A. degree in physics and the M.S. degree in electrical engineering in 1998 and 2001, respectively, from the University of California at Berkeley, where she is currently working toward the Ph.D. degree in electrical engineering.

Her research interests include single-mode and multimode optical fiber communications and free-space optical communications.

Joseph M. Kahn (M'90–SM'98–F'00) received the A.B., M.A., and Ph.D. degrees in physics from the University of California at Berkeley in 1981, 1983, and 1986, respectively.

He is currently a Professor in the Department of Electrical Engineering at Stanford University, Stanford, CA. Previously, he was a Professor in the Department of Electrical Engineering and Computer Sciences at University of California at Berkeley. In 2000, he co-founded StrataLight Communications, Inc., where he is currently Chief Scientist. From 1987 to 1990, he was a Member of Technical Staff in the Lightwave Communications Research Department of AT&T Bell Laboratories, where he performed research on multi-gigabit-per-second coherent optical fiber transmission systems, setting several world records for receiver sensitivity. His current research interests include wireless communication using antenna arrays, free-space optical communication, optical fiber communication, and wireless communication for networks of sensors based on micro-electromechanical systems.

Dr. Kahn received the National Science Foundation Presidential Young Investigator Award in 1991. He is a member of the IEEE Communications Society, the IEEE Information Theory Society, and the IEEE Lasers and Electro-Optics Society. From 1993 to 2000, he served as a technical editor of *IEEE Personal Communications Magazine*.